Self-Assembling Asymmetric Bisphenazines with Tunable Electronic Properties

Dong-Chan Lee,* Kyoungmi Jang, Kelly K. McGrath, Rycel Uy, Kathleen A. Robins, and David W. Hatchett

Department of Chemistry, University of Nevada Las Vegas, 4505 Maryland Parkway, Box 454003, Las Vegas, Nevada 89154-4003

Received February 21, 2008

This paper reports novel self-assembling T-shaped conjugated molecules based on asymmetric bisphenazines in which hexadecyloxy substituted bisphenazine is orthogonally fused with 1,4-bis(2-phenylethynyl)benzene. Tunability of one-dimensional (1D) self-assembly and electronic properties of the system was demonstrated by peripheral substitution with small functional groups. These functional groups (OCH_3, H, CN) progressively reduced LUMO levels as predicted by theoretical calculations and experimentally verified by cyclic voltammetry (CV). Furthermore, the morphologies of 1D assembly were greatly influenced by the substituents. While conformational flexibility of methoxy hampered successful assembly, hydrogen and cyano substitution induced the formation of rigid microstrands and flexible nanofibers, respectively, using phase transfer methods. Detailed instrumental analyses of the 1D assembled clusters including scanning electron microscopy (SEM), differential scanning calorimetry (DSC), and X-ray diffraction (XRD) are presented. The design strategy of the new T-π-core and peripheral substitution provides a tool to control the morphology of 1D clusters with minimal structural modification of the π-core while allowing modulation of electronic properties.

Introduction

Current demands in the area of organic semiconductor design focus on both electronic properties and self-assembling ability in order to create well-defined nanostructures. Various design strategies and assembly methodologies have been reported that successfully induce self-assembly of π-conjugated compounds, with systems ranging from small molecules to polymers.[1] One-dimensional (1D) self-assemblies of organic semiconductors, including nanofibers,[2] nanobelts,[3] and nanotubes,[4] have been particularly useful in preparing high-aspect-ratio nanoclusters through intermolecular $\pi-\pi$ interaction and ultimately achieving high levels of supramolecular organization. These 1D nanoclusters have excellent potential for the future of nanodevice fabrication, as single nanofiber and nanowire devices have already been demonstrated.[2b,5] Although proper assembly processes are indispensable, a key component for inducing 1D assembly is strategic molecular engineering. Current design techniques employ either symmetric[2,3a,b,d–f,4a–d] or asymmetric π-cores[4e,6] with solubilizing alkyl substituents. The morphology of self-assembled clusters is frequently controlled by side group manipulation, including use of nonidentical side groups with opposite polarities.[2f,g3f,4b–e]

Despite the advances in the molecular design of organic semiconductors, the majority are electron-donating (p-type)

* Corresponding author. E-mail: Dong-Chan.Lee@unlv.edu.

(1) (a) Hoeben, F. J. M.; Jonkheijm, P.; Meijer, E. W.; Schenning, A. P. H. J. *Chem. Rev.* **2005**, *105*, 1491–1546. (b) Schenning, A. P. H. J.; Meijer, E. W. *Chem. Commun.* **2005**, 3245–3258. (c) Grimsdale, A. C.; Müllen, K. *Angew. Chem., Int. Ed.* **2005**, *44*, 5592–5629.

(2) (a) Kastler, M.; Pisula, W.; Wasserfallen, D.; Pakula, T.; Müllen, K. *J. Am. Chem. Soc.* **2005**, *127*, 4286–4296. (b) Xiao, S.; Tang, J.; Beetz, T.; Guo, X.; Tremblay, N.; Siegrist, T.; Zhu, Y.; Steigerwald, M.; Nuckolls, C. *J. Am. Chem. Soc.* **2006**, *128*, 10700–10701. (c) Balakrishnan, K.; Datar, A.; Zhang, W.; Yang, X.; Naddo, T.; Huang, J.; Zuo, J.; Yen, M.; Moore, J. S.; Zang, L. *J. Am. Chem. Soc.* **2006**, *128*, 6576–6577. (d) Naddo, T.; Che, Y.; Zhang, W.; Balakrishnan, K.; Yang, X.; Yen, M.; Zhao, J.; Moore, J. S.; Zang, L. *J. Am. Chem. Soc.* **2007**, *129*, 6978–6979. (e) Puigmartí-Luis, J.; Laukhin, V.; del Pino, Á. P.; Vidal-Gancedo, J.; Rovira, C.; Laukhina, E.; Amabilino, D. B. *Angew. Chem., Int. Ed.* **2007**, *46*, 238–241. (f) Hong, D.-J.; Lee, E.; Lee, M. *Chem. Commun.* **2007**, *180*, 1–1803. (g) Hamaoui, B. E.; Zhi, L.; Pisula, W.; Kolb, U.; Wu, J.; Müllen, K. *Chem. Commun.* **2007**, 2384–2386.

(3) (a) Balakrishnan, K.; Datar, A.; Oitker, R.; Chen, H.; Zuo, J.; Zang, L. *J. Am. Chem. Soc.* **2005**, *127*, 10496–10497. (b) Balakrishnan, K.; Datar, A.; Naddo, T.; Huang, J.; Oitker, R.; Yen, M.; Zhao, J.; Zang, L. *J. Am. Chem. Soc.* **2006**, *128*, 7390–7398. (c) Jiang, H.; Sun, X.; Huang, M.; Wang, Y.; Li, D.; Dong, S. *Langmuir* **2006**, *22*, 3358–3361. (d) Datar, A.; Oitker, R.; Zang, L. *Chem. Commun.* **2006**, 1649–1651. (e) Che, Y.; Datar, A.; Yang, X.; Naddo, T.; Zhao, J.; Zang, L. *J. Am. Chem. Soc.* **2007**, *129*, 6354–6355. (f) Che, Y.; Datar, A.; Balakrishnan, K.; Zang, L. *J. Am. Chem. Soc.* **2007**, *129*, 7234–7235. (g) Guo, S.; Dong, S.; Wang, E. *Chem. Mater.* **2007**, *19*, 4621–4623.

(4) (a) Kimizuka, N.; Kawasaki, T.; Hirata, K.; Kunitake, T. *J. Am. Chem. Soc.* **1995**, *117*, 6360–6361. (b) Hill, J. P.; Jin, W.; Kosaka, A.; Fukushima, T.; Ichihara, H.; Shimomoura, T.; Ito, K.; Hashizume, T.; Ishii, N.; Aida, T. *Science* **2004**, *304*, 1481–1483. (c) Yamamoto, Y.; Fukushima, T.; Suna, Y.; Ishii, N.; Saeki, A.; Seki, S.; Tagawa, S.; Taniguchi, M.; Kawai, T.; Aida, T. *Science* **2006**, *314*, 1761–1764. (d) Yamamoto, T.; Fukushima, T.; Yamamoto, Y.; Kosaka, A.; Jin, W.; Ishii, N.; Aida, T. *J. Am. Chem. Soc.* **2006**, *128*, 14337–14340. (e) Kim, J.-K.; Lee, E.; Lee, M. *Angew. Chem., Int. Ed.* **2006**, *45*, 7195–7198.

(5) Briseno, A. L.; Mannsfeld, S. C. B.; Lu, X.; Xiong, Y.; Jenekhe, S. A.; Bao, Z.; Xia, Y. *Nano Lett.* **2007**, *7*, 668–675.

(6) (a) Kumar, S.; Manickam, M. *Mol. Cryst. Liq. Cryst.* **2000**, *338*, 175–179. (b) Date, R. W.; Bruce, D. W. *J. Am. Chem. Soc.* **2003**, *125*, 9012–9013. (c) Kouwer, P. H. J.; Jager, W. F.; Mijs, W. J.; Picken, S. J. *J. Mater. Chem.* **2003**, *13*, 458–469. (d) Foster, E. J.; Babuin, J.; Nguyen, N.; Williams, V. E. *Chem. Commun.* **2004**, 2052–2053. (e) Kouwer, P. H. J.; Mehl, G. H.; Picken, S. J. *Mol. Cryst. Liq. Cryst.* **2004**, *411*, 387–396.

10.1021/cm800521p CCC: $40.75
Published on Web 05/08/2008

with only a limited number characterized as electron-accepting (n-type). Examples of n-type semiconductors that have been used successfully as optoelectronic active materials include perylenediimide,[7] C_{60},[8] diphenylanthrazolines,[9] conjugated ladder polymers,[10] etc. Clearly, n-type semiconductors are equally as important when compared to their p-type counterparts since they are vital constituents for donor/acceptor organic solar cells and complementary circuits. Consequently, developing useful n-type semiconductors is a central focus of our research. A primary objective in our molecular design is to create a material with a large electron affinity while maintaining the desired self-assembling properties. Incorporation of desired electron-affinity while allowing self-assembly requires sensible molecular design strategies. One approach used to create n-type semiconductors involves incorporating electron-withdrawing functional groups into p-type structural analogues.[11] Although the necessary electronic-deficiencies can be achieved using this strategy, self-assembly of these systems are limited. Employing heteroaromatic moieties such as pyridine, pyrazine, triazine, etc.[12] is an alternative for achieving electron-deficiency owing to the presence of the electron-withdrawing imine nitrogens.[13] The latter approach is preferable given that properly designed large fused aromatic heterocyclics can promote self-assembly.[14]

In this paper, we report the synthesis and characterization of new n-type semiconductors that are based on asymmetric bisphenazines and designed to have tunable electronic and 1D self-assembling properties. Bisphenazine is an excellent π-core platform for both self-assembly and electron-deficiency as exemplified by a previous report which demonstrated liquid crystallinity and possible utility as an electron transporting material.[15] However, it is important to note that little is known about the synthesis and the influence of chemical modifications on bisphenazine.

The structural features of our target molecules merit further elaboration: (i) π-Conjugated cores are T-shaped, in which electron-deficient bisphenazine (vertical line) is fused orthogonally to 1,4-bis(2-phenylethynyl)benzene (horizontal line). Our theoretical calculations revealed that the π-core adopts a planar geometry which promotes self-assembly. Additionally, the feasibility of chemical modification at the phenyl ring at both ends of the horizontal line of the T-shaped π-core provides an opportunity to further tune the electronic properties. (ii) The long hexadecyloxy side groups at the end of the vertical line of the T-cores promote solubility in common organic solvents and assist self-assembly through cooperative van der Waals interaction. The unparalleled design platform presented in this work consists of three crucial components: an asymmetric π-core, hexadecyloxy side groups, and electronic property tuning substituents. Each of these components plays a unique role in the assembling ability and the electronic character of the whole molecules. Of critical importance is the harmonious interplay between all three components, allowing 1D assembly while modulating the electronic properties of the π-core. It was found that peripheral modification of the π-core with small, seemingly trivial size electronic property tuning substituents (OCH_3, H, CN) greatly influenced the morphology of the 1D assembly. Although the conformational flexibility of OCH_3 prevented the formation of organized clusters, H and CN substitution allowed successful 1D assembly with a remarkable difference in the morphology. Herein, we present

(7) (a) Schmidt-Mende, L.; Fechtenkötter, A. F.; Müllen, K.; Moons, E.; Friend, R. H.; MacKenzie, J. D. *Science* **2001**, *293*, 1119–1122. (b) Hänsel, H.; Zettl, H.; Krausch, G.; Kisselev, R.; Thelakkat, M.; Schmidt, H.-W. *Adv. Mater.* **2003**, *15*, 2056–2060. (c) Tatemichi, S.; Ichikawa, M.; Koyama, T.; Taniguchi, Y. *Appl. Phys. Lett.* **2006**, *89*, 112108−1112108−3. (d) Pandey, A. K.; Dabos-Seignon, S.; Nunzi, J.-M. *Appl. Phys. Lett.* **2006**, *89*, 113506−1113506−2. (e) Briseno, A. L.; Tseng, R. J.; Li, S.-H.; Chih, C.-W.; Yang, Y.; Falcao, E. H. L.; Wudl, F.; Ling, M.-M.; Chen, H. Z.; Bao, Z.; Meng, H.; Kloc, C. *Appl. Phys. Lett.* **2006**, *89*, 222111−1222111−3. (f) Ling, M.-M.; Bao, Z.; Erk, P.; Koenemann, M.; Gomez, M. *Appl. Phys. Lett.* **2007**, *90*, 093508−1093508−3. (g) Briseno, A. L.; Mannsfeld, S. C. B.; Reese, C.; Hancock, J. M.; Xiong, Y.; Jenekhe, S. A.; Bao, Z.; Xia, Y. *Nano Lett.* **2007**, *7*, 2847–2853.

(8) (a) Yu, G.; Gao, J.; Hummelen, J. C.; Wudl, F.; Heeger, A. J. *Science* **1995**, *270*, 1789–1791. (b) Peumans, P.; Uchida, S.; Forrest, S. R. *Nature* **2003**, *425*, 158–162. (c) Xue, J.; Uchida, S.; Rand, B. P.; Forrest, S. R. *Appl. Phys. Lett.* **2004**, *84*, 3013–3015. (d) Uchida, S.; Xue, J.; Rand, B. P.; Forrest, S. R. *Appl. Phys. Lett.* **2004**, *84*, 4218–4220. (e) Rand, B. P.; Xue, J.; Uchida, S.; Forrest, S. R. *J. Appl. Phys.* **200598**, 124902−1124902−7. (f) Xue, J.; Rand, B. P.; Uchida, S.; Forrest, S. R. *J. Appl. Phys.* **2005**, *98*, 124903−1124903−9.

(9) Tonzola, C. J.; Alam, M. M.; Kaminsky, W.; Jenekhe, S. A. *J. Am. Chem. Soc.* **2003**, *125*, 13548–13558.

(10) (a) Babel, A.; Jenekhe, S. A. *Adv. Mater.* **2002**, *14*, 371–374. (b) Babel, A.; Jenekhe, S. A. *J. Am. Chem. Soc.* **2003**, *125*, 13656–13657. (c) Babel, A.; Wind, J. D.; Jenekhe, S. A. *Adv. Funct. Mater.* **2004**, *14*, 891–898. (d) Alam, M. M.; Jenekhe, S. A. *Chem. Mater.* **2004**, *16*, 4647–4656.

(11) (a) Halls, J. J. M.; Walsh, C. A.; Greenham, N. C.; Marseglia, E. A.; Friend, R. H.; Moratti, S. C.; Homes, A. B. *Nature* **1995**, *376*, 498–500. (b) Granström, M.; Petritsch, K.; Arias, A. C.; Lux, A.; Andersson, M. R.; Friend, R. H. *Nature* **1998**, *395*, 257–260. (c) Gao, J.; Yu, G.; Heeger, A. J. *Adv. Mater.* **1998**, *10*, 692–695. (d) Moratti, S. C.; Cervini, R.; Holmes, A. B.; Baigent, D. R.; Friend, R. H.; Greenham, N. C.; Grüner, J.; Hamer, P. J. *Synth. Met.* **1995**, *71*, 2117–2120. (e) Baigent, D. R.; Marks, R. N.; Greenham, N. C.; Friend, R. H.; Moratti, S. C.; Holmes, A. B. *Synth. Met.* **1995**, *71*, 2177–2178. (f) Peng, Z.; Galvin, M. E. *Chem. Mater.* **1998**, *10*, 1785–1788. (g) Bao, Z.; Lovinger, A. J.; Brown, J. *J. Am. Chem. Soc.* **1998**, *120*, 207–208. (h) Sakamoto, Y.; Suzuki, T.; Miura, A.; Fujikawa, H.; Tokito, S.; Taga, Y. *J. Am. Chem. Soc.* **2000**, *122*, 1832–1833. (i) Heidenhain, S. B.; Sakamoto, Y.; Suzuki, T.; Miura, A.; Fujikawa, H.; Mori, T.; Tokito, S.; Taga, Y. *J. Am. Chem. Soc.* **2000**, *122*, 10240–10241. (j) Sakamoto, Y.; Komatsu, S.; Suzuki, T. *J. Am. Chem. Soc.* **2001**, *123*, 4643–4644. (k) Yassar, A.; Demanze, F.; Jaafari, A.; Idrissi, M. E.; Coupry, C. *Adv. Funct. Mater.* **2002**, *12*, 699–708. (l) Pappenfus, T. M.; Burand, M. W.; Janzen, D. E.; Mann, K. R. *Org. Lett.* **2003**, *5*, 1535–1538. (m) Facchetti, A.; Yoon, M.-H.; Stern, C. L.; Katz, H. E.; Marks, T. J. *Angew. Chem., Int. Ed.* **2003**, *42*, 3900–3903.

(12) (a) Kulkarni, A. P.; Tonzola, C. J.; Babel, A.; Jenekhe, S. A. *Chem. Mater.* **2004**, *16*, 4556–4573. (b) Karastatiris, P.; Mikroyannidis, J. A.; Spiliopoulos, I. K.; Kulkarni, A. P.; Jenekhe, S. A. *Macromolecules* **2004**, *37*, 7867–7878. (c) Kulkarni, A. P.; Zhu, Y.; Jenekhe, S. A. *Macromolecules* **2005**, *38*, 1553–1563. (d) Tonzola, C. J.; Alam, M. M.; Jenekhe, S. A. *Macromolecules* **2005**, *38*, 9539–9547.

(13) Yamamoto, T.; Maruyama, T.; Zhou, Z.; Ito, T.; Fukuda, T.; Yoneda, Y.; Begamn, F.; Ikeda, T.; Sasaki, S.; Takezoe, H.; Fukuda, A.; Kubota, K. *J. Am. Chem. Soc.* **1994**, *116*, 4832–4845.

(14) (a) Keinan, E.; Kumar, S.; Singh, S. P.; Ghirlando, R.; Wachtel, E. J. *Liq. Cryst.* **1992**, *11*, 157–173. (b) Kumar, S.; Wachtel, E. J.; Keinan, E. *J. Org. Chem.* **1993**, *58*, 3821–3827. (c) Kumar, S.; Rao, D. S. S.; Prasad, S. K. *J. Mater. Chem.* **1999**, *9*, 2751–2754. (d) Lemaur, V.; da Silva Filho, D. A.; Coropceanu, V.; Lehmann, M.; Geerts, Y.; Piris, J.; Debije, M. G.; van de Craats, A. M.; Senthilkumar, K.; Siebbeles, L. D. A.; Warman, J. M.; Brédas, J.-L.; Cornil, J. *J. Am. Chem. Soc.* **2004**, *126*, 3271–3279. (e) Kadam, J.; Faul, C. F. J.; Scherf, U. *Chem. Mater.* **2004**, *16*, 3867–3871. (f) Ishi-I, T.; Yaguma, K.; Kuwahara, R.; Taguri, Y.; Mataka, S. *Org. Lett.* **2006**, *8*, 585–588.

(15) Hu, J.; Zhang, D.; Jin, S.; Cheng, S. Z. D.; Harris, F. W. *Chem. Mater.* **2004**, *16*, 4912–4915.

Scheme 1. Synthetic Approaches to Intermediate 2

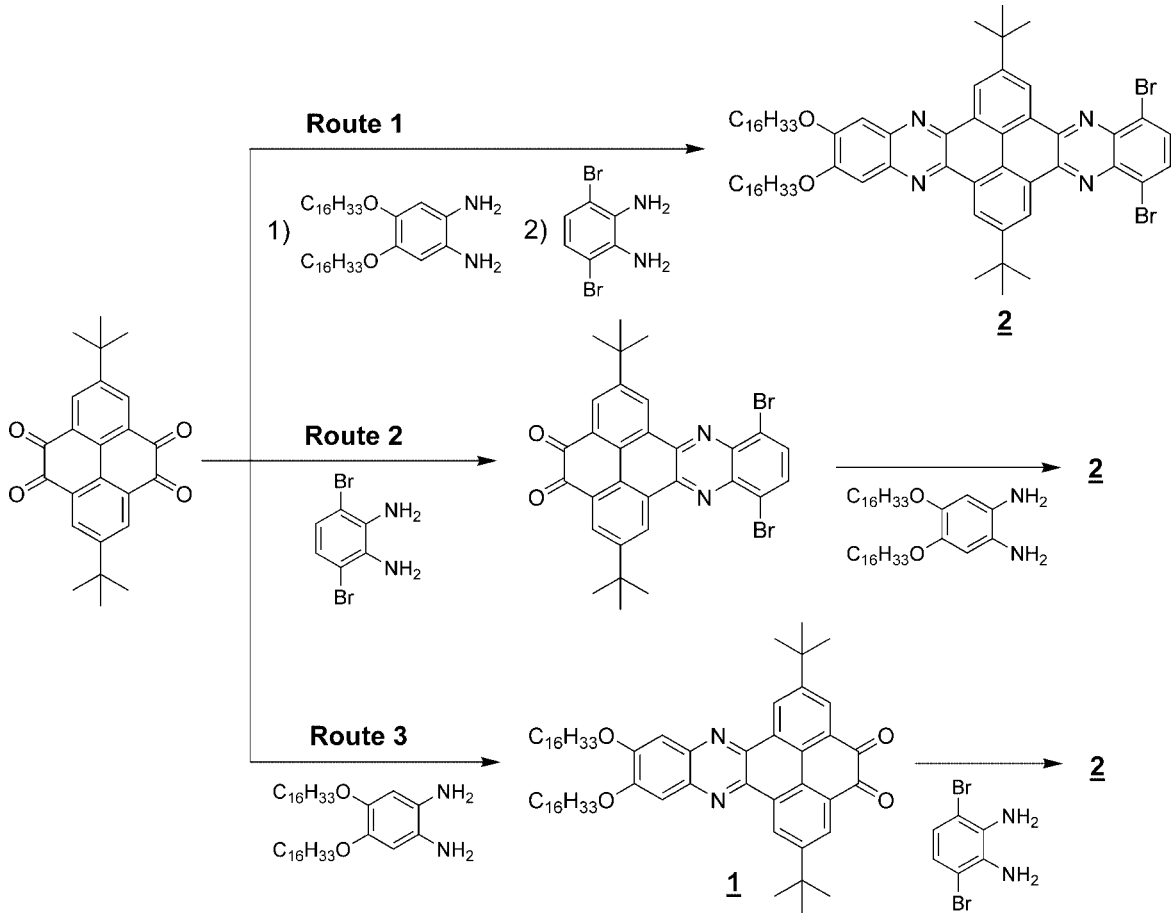

synthetic details and spectroscopic investigation on physical properties and morphological behaviors of these T-shaped molecules.

Results and Discussion

Synthesis. The target molecules (**5a**−**c**) were prepared by the procedure shown in Schemes 1 and 2. Efficient synthetic route to the key intermediate, compound **2**, was established through three different approaches as shown in Scheme 1.

The first was a simple sequential addition of 1,2-bishexadecyloxy-4,5-diaminobenzene to 2,7-di-*tert*-butylpyrene-4,5,9,10-tetraone followed by 1,4-dibromo-2,3-diaminobenzene without any purification of diketophenazine intermediate (Route 1 in Scheme 1). Although this reaction procedure had the least number of steps, it resulted in a low yield, presumably because of initial side products at the first cyclization, which later caused improper stoichiometry at the second cyclization. The second approach (Route 2) was a stepwise cyclization beginning with 1,4-dibromo-2,3-diaminobenzene and the tetraone including the purification of the resultant diketophenazine intermediate. However, this intermediate was only sparingly soluble in organic solvents hampering purification. As a result, subsequent cyclization with 1,2-bishexadecyloxy-4,5-diaminobenzene resulted in a low yield. Finally, compound **2** was obtained in high yield by the stepwise cyclization of 1,2-bishexadecyloxy-4,5-diaminobenzene to the tetraone followed by 1,4-dibromo-2,3-diaminobenzene (Route 3). Unlike the diketophenazine intermediate in Route 2, the intermediate in Route 3 contains hexadecyloxy substituents that rendered good solubility in common organic solvents, making purification feasible.

The title compounds **5a**−**c** could be prepared by Sonogashira coupling[16] of compound **2** and the corresponding arylene ethynylenes; however, we chose the cross coupling between compound **4** and iodoarenes because of the higher reactivity of iodoarenes toward Sonogashira coupling reaction than bromoarenes. In addition, compound **4** can be reacted directly with commercially available iodoarenes to afford compounds **5a**−**c**, whereas more synthetic steps are required to prepare three different arylene ethynylenes. Hence, the best strategy for the synthesis of **5a**−**c** is the coupling between **4** and various iodo compounds. The first attempt to couple trimethylsilylacetylene (TMSA) (**3**) to compound **2** employing the $Pd(PPh_3)_2Cl_2$ catalyst produced the monosubstituted bisphenazine with TMSA as a major product in addition to unreacted **2**. To increase the reactivity, we can prepare the diiodo-version of compound **2**. However, the precursor, 1,4-diiodo-2,3-diaminobenzene, requires three additional synthetic steps from 1,4-dibromo-2,3-diaminobenzene.[17] Instead, we found that $Pd(OAc)_2$ dramatically improved the yield for the coupling of TMSA to compound

(16) (a) Sonogashira, K.; Tohda, Y.; Hagihara, N. *Tetrahedron Lett.* **1975**, *50*, 4467–4470. (b) Takahashi, S.; Kuroyama, Y.; Sonogashira, K.; Hagihara, N. *Synthesis* **1980**, 627–630. (c) Chinchilla, R.; Nájera, C. *Chem. Rev.* **2007**, *107*, 874–922.

(17) Tsubata, Y.; Suzuki, T.; Miyashi, T. *J. Org. Chem.* **1992**, *57*, 6749–6755.

Scheme 2. Synthetic Routes to T-Shaped Molecules (5a−c)

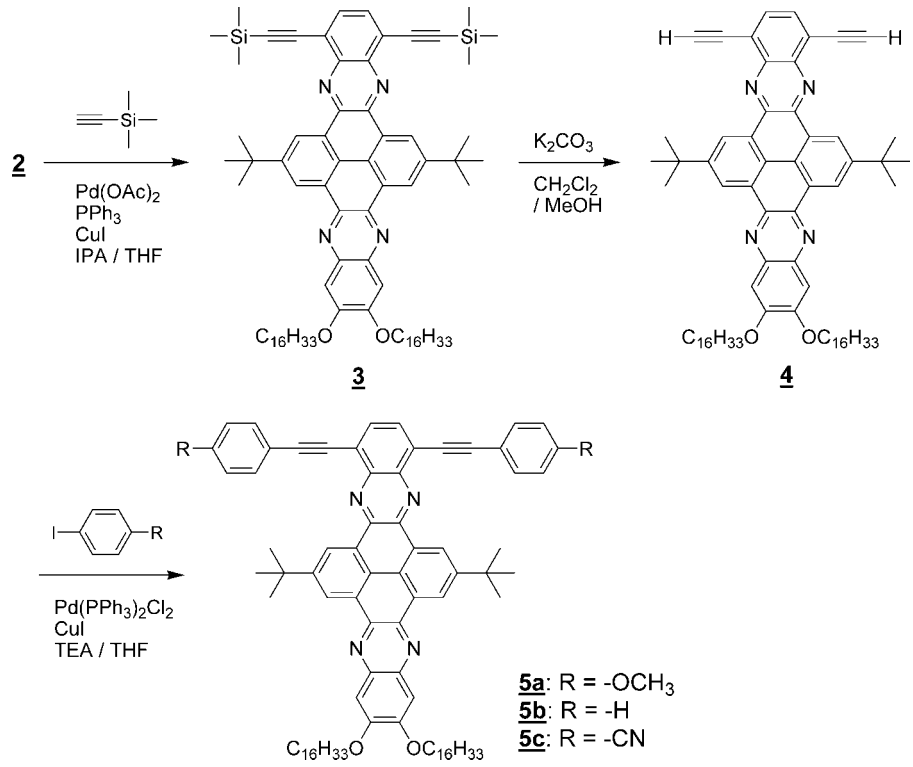

2 (95%). After removal of the TMS protecting groups by K_2CO_3, **5a**−**c** were obtained by Sonogashira coupling with the relevant iodoarenes and $Pd(PPh_3)_2Cl_2$ under typical Sonogashira coupling conditions. Compounds **5b** and **5c** were obtained with good yields, 83 and 85%, respectively. On the other hand, **5a** gave a low yield (15%) with a number of unidentifiable side products. All of the compounds were soluble in common organic solvents such as chloroform, methylene chloride, and THF, enabling meaningful structural and physical property characterizations.

Optical and Electrochemical Properties and Theoretical Calculation. UV−vis absorption spectra of **5a**−**c** were recorded in chloroform solution at 5×10^{-6} mol/L. As shown in Figure 1, the absorption spectra of **5a**−**c** show similar patterns that have λ_{max} at ca. 400 and 422 nm with a shoulder at ca. 450 nm.

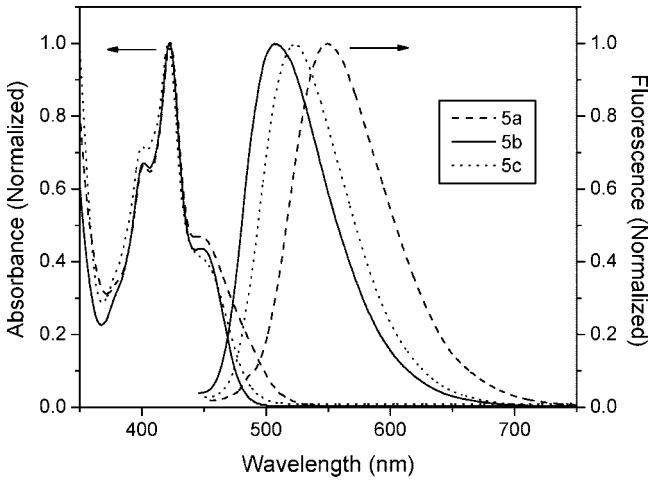

Figure 1. Normalized UV−vis and fluorescence spectra of compounds **5a**−**c** in chloroform. The excitation wavelength for fluorescence is 420 nm.

All the peaks followed Beer's law, which confirms that the absorptions are intrinsic to molecules rather than aggregation. The peaks at 400 and 422 nm originate from the bisphenazine ring, whereas the absorbance at ca. 450 nm is attributed to the extension of conjugation through arylene-ethynylene substituents. From the slope of Beer's plot, the extinction coefficient at 422 nm were 4.9×10^4 L mol^{-1} cm^{-1} for **5a**, 6.2×10^4 L mol^{-1} cm^{-1} for **5b**, and 6.8×10^4 L mol^{-1} cm^{-1} for **5c**. The absorption edges in the spectra progressively shifted to lower energy as the peripheral substituent changed from H (**5b**) to CN (**5c**) to OCH_3 (**5a**). Accordingly, the HOMO−LUMO energy gap of **5b**, **5c**, and **5a**, calculated from the tangent of the absorption edge,[18] decreased from 2.55 to 2.50 to 2.41 eV.

A similar behavior was observed in the emission spectra measured in chloroform solution. The emission maximums were 507, 524, and 549 nm for **5b**, **5c**, and **5a**, respectively, with 422 nm as the excitation wavelength.

The influence of substituent groups on the reduction of the series of molecules was examined using CV. The voltammetry of species **5a**−**c** are shown in Figure 2.

For a reversible system, one would expect peak splitting to be Nernstian with $\Delta E_p = E_{pc} - E_{pa} = 59$ mV/n, where n is the number of electrons transferred. In contrast, for quasi-reversible systems the peak splitting is a function of the scan rate ν, the rate constant for electron exchange $k°$, and the transfer coefficient α, which is based on the reaction energy barrier.[19] The splitting for quasi-reversible systems is therefore larger with values of $\Delta E_p \geq 90$ mV/n. The data

(18) Bundgaard, E.; Krebs, F. C. *Macromolecules* **2006**, *39*, 2823–2831.
(19) Bard, A. J.; Faulkner L. R. In *Electrochemical Methods: Fundamentals and Applications*, 2nd ed.; John Wiley and Sons Inc.: New York, 2001; pp 242−243.

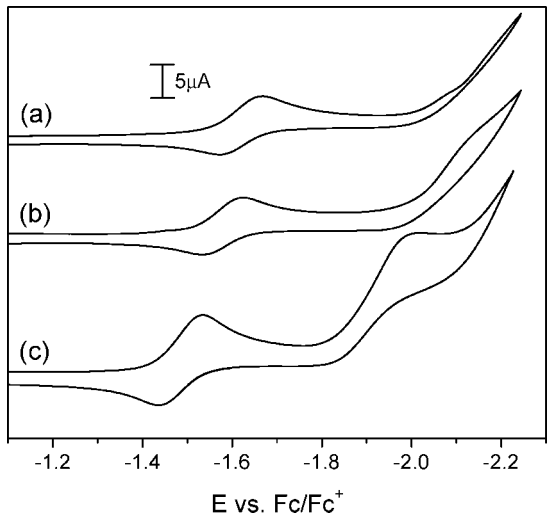

Figure 2. Cyclic voltammograms for the reduction of (a) **5a**, (b) **5b**, and (c) **5c**. Scan rate = 100 mV/s.

for **5a**, **5b**, and **5c** was characterized by quasi-reversible voltammetric waves with peak splitting on the order of 100 mV for all three molecules. In addition, the cathodic current was larger than the anodic current with $i_{pc}/i_{pa} = 1.40$, 1.51, and 1.39 for **5a**, **5b**, and **5c**, respectively. The data indicate that the first reduction for all the compounds is energetically more favorable than the subsequent oxidation. The resolution of a second one-electron reduction was observed for only **5c**, consistent with higher electron affinity for the molecule. **5c** contains electron-withdrawing cyano, which makes the reduction more energetically favorable in comparison to **5b** with neutral hydrogen or **5a** with electron-donating methoxy. Therefore, the potentials associated with the first reduction are indicative of the ease of reduction with E_{pc} values for **5c** < **5b** < **5a**. The onset potential for the reduction can also be used to provide information regarding the electronic energy levels as a function of the substituent groups used to modulate electronic properties. Previous studies have shown that similarly structured electron-deficient molecules can be reduced through two one-electron processes, which provide information regarding the LUMO.[20] In this analysis, the onset potentials for each molecule were determined for the first reduction wave. These values are provided in Table 1 with the calculated LUMO energies. We were unable to resolve accurate oxidation potentials of **5a**−**c** because of overlap with the solvent background. Therefore, direct estimation of HOMO energies from the oxidation potentials was not possible. Instead, HOMO energies associated with the molecules with different functional groups were estimated from the LUMO energies in combination with the HOMO−LUMO gaps derived from the optical studies.[20]

To further evaluate the electronic properties of compounds **5a**, **5b**, and **5c**, theoretical calculations were carried out on all three systems. HOMO and LUMO energies predicted by single point B3LYP/6-31+G*//B3LYP/6-31G* were in reasonable agreement when compared with experiment values. It is interesting to note that compound **5c** produced the best agreement between theoretical and experimental findings, with a difference of 0.06 eV in the HOMO energy and 0.18 eV in the LUMO energy. The theoretically predicted HOMO−LUMO energy gaps were overestimated by 0.24−0.29 eV for all three molecules when compared with experimental values. The HOMO and LUMO orbitals for all three compounds are presented in Figure 3.

There is an obvious similarity between **5a** and **5b**, with the distribution of both the highest occupied and the lowest unoccupied orbitals localized on the horizontal line of the T-cores. The disparity in the HOMO orbital of **5c** arises from extremely close HOMO and HOMO-1 energies, with the HOMO-1 orbital localized in an equivalent manner to the HOMO orbitals for **5a** and **5b**. An initial, low-level CIS analysis found that the first electronic energy excitation for **5c** is predicted to be between the HOMO-1 and LUMO orbitals. Consequently, all three compounds can be viewed as having equivalent transitions of equivalent states. All the energy values from electrochemistry and theoretical calculation are provided in Table 1 for comparison.

Self-Assembly, Thermal Properties, and X-ray Diffraction. The 1D assembly of nanostructures can be induced through various methods such as precipitation,[3c,g] spin-casting,[2a,d] injection,[3a,21] solvent vapor annealing,[3b,d] or solvent exchange processes.[2g,3b,e,f,7g] In this study, the self-assembly of compounds **5a**−**c** was investigated through a phase transfer method in which the molecules in solution experience solubility change during a slow diffusion of a poor solvent into the solution and thus initiates assembly. Using the phase transfer method requires an optimum polarity modulation between good and poor solvent such that two solvent phases can be maintained at the nucleation stage of assembly, and then slow diffusion to each other at the growth stage. Furthermore, the concentration and the ratio of poor to good solvent plays an additional, critical role in obtaining well-defined 1D nanostructures. We found that the initial optimized conditions for 1D assembly were determined to be 0.6 mM of asymmetric bisphenazine (**5a**−**c**) in methylene chloride to which 40 vol% of methanol was slowly added to maintain two phases. These mixtures were left undisturbed overnight. Despite the fact that the assemblies could be induced with lower ratios of methanol, the asymmetric bisphenazine retained significant solubility in the binary solvent system, allowing for the nanostructures to be redissolved into solution. In contrast, when the solvent ratio of methanol is too high, fast molecular aggregation is predominant prohibiting delicate 1D growth. Note that a methylene chloride/*n*-hexane binary solvent system with 40 vol% of *n*-hexane did not induce 1D self-assembly, although *n*-hexane is a poor solvent to the asymmetric bisphenazines. Compounds **5b** and **5c** were assembled successfully by the optimized condition producing 1D clusters; however, **5a** produced only a cloudy suspension under the same condition. As predicted by theoretical modeling, the fact that **5a** could not induce assembly is due to the free rotation of methoxy groups, which interferes with effective molecular packing. To identify the morphology of the assembled clusters, we

(20) Fogel, Y.; Kastler, M.; Wang, Z.; Andrienko, D.; Bodwell, G. J.; Müllen, K. *J. Am. Chem. Soc.* **2007**, *129*, 11743–11479.

(21) Vriezema, D. M.; Kros, A.; de Gelder, R.; Cornelissen, J. J. L. M.; Rowan, A. E.; Nolte, R. J. M. *Macromolecules* **2004**, *37*, 4736–4739.

Table 1. Summary of Electronic Properties of 5a−c from Experiments and Theoretical Calculation

compd	E_{red}^{peak} (V)	E_{red}^{onset} (V)	E_{LUMO}[a] (eV)	E_{HOMO}[b] (eV)	E_{gap}[c] (eV)	E_{LUMO}[d] (eV)	E_{HOMO}[d] (eV)	E_{gap}[d] (eV)
5a	−1.67	−1.54	−3.26	−5.67	2.41	−2.54	−5.22	2.68
5b	−1.62	−1.51	−3.29	−5.84	2.55	−2.69	−5.53	2.84
5c	−1.53	−1.42	−3.38	−5.88	2.50	−3.20	−5.94	2.74

[a] $E_{LUMO} = -(E_{red}^{onset} + 4.8\ eV)$. [b] $E_{HOMO} = E_{LUMO} - E_{gap}^{optical}$. [c] Optical HOMO−LUMO energy gap. [d] Theoretical calculation.

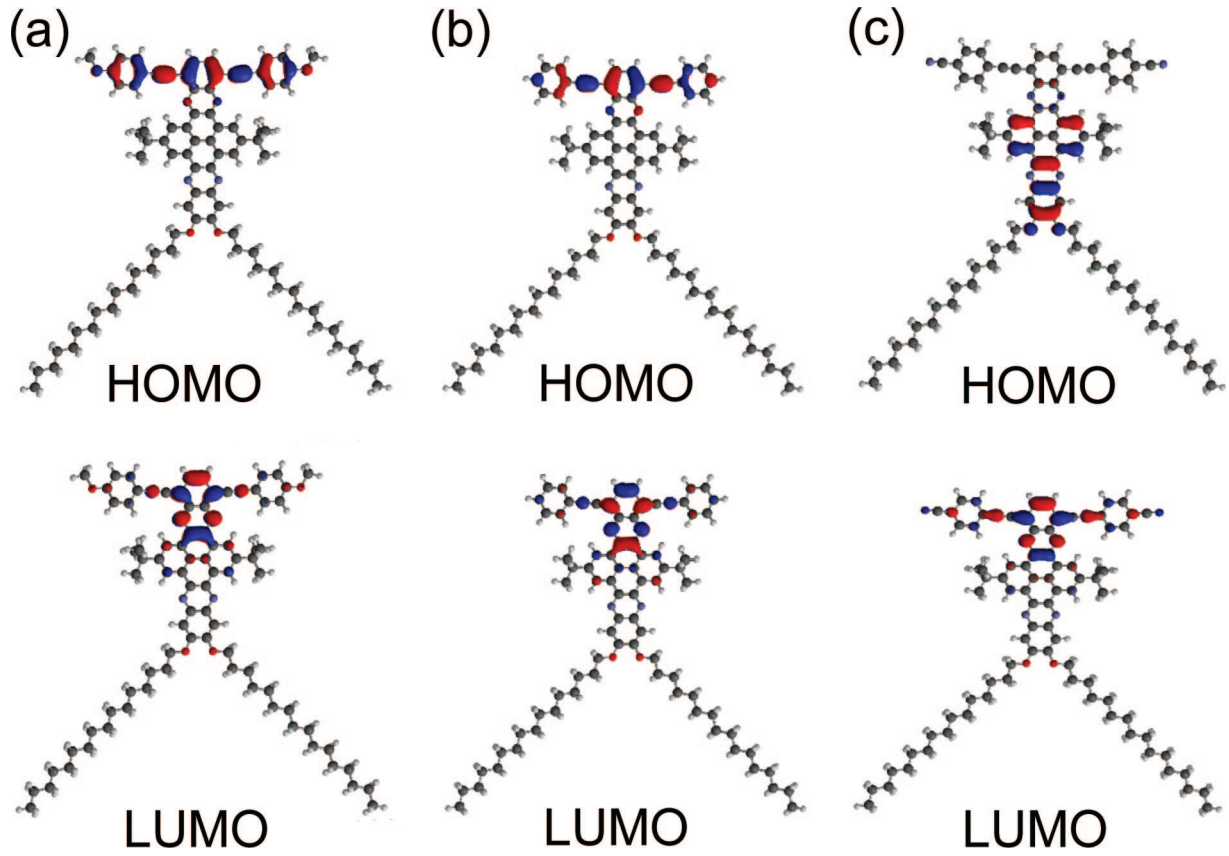

Figure 3. HOMO and LUMO orbitals of (a) **5a**, (b) **5b**, and (c) **5c** predicted using optimized geometries at the B3LYP/6−31G* level of theory.

conducted SEM experiments. The excess solvent was removed by pipetting, and the assembled clusters were then transferred to a clean gold/mica substrate.

As shown in Figure 4, well-defined structures were obtained with compounds **5b** and **5c**. The morphology of the assembled clusters from **5b** and **5c** showed striking differences. Compound **5b** assembled into high aspect ratio straight strand-like clusters in microscale width with random distribution in the width (Figure 4a−c). The length of the longest microstrand reached over 4 mm. On the contrary, flexible 1D nanofibers were formed from compound **5c** (Figure 4d−f). Single and bundles of fibers were observed with individual fiber thickness of ca. 140 nm. From the texture of the fibers with larger thickness, it was clear that small fibers aggregated to form bundles. Unlike the microstrands of **5b**, the nanofibers of **5c** showed a fairly homogeneous thickness distribution. These flexible and endless fibers formed a 3D network reminiscent to fiber networks typically observed from organogels.[22]

Thermal properties of self-assembled clusters of **5b** and **5c** were investigated by DSC (Figures 5 and 6). As a comparison, simple precipitates were prepared by adding excess methanol to concentrated solutions of **5b** and **5c** in methylene chloride at once. Three heating and cooling scans were conducted with a rate of 10 °C/min to test the reproducibility of thermal behaviors.

The precipitate of **5b** showed two endotherms at 204.5 and 247.7 °C with heat of melting of 4.9 and 21.6 J/g, respectively. These endothermic transitions were reproducible up to three heating/cooling scans. However, microstrands of **5b** displayed complex thermal behaviors by showing two additional endotherms plus those observed from the precipitate; 109.8 °C (25.6 J/g) and 136.7 °C (31.4 J/g). The additional two endotherms at lower temperature were obviously the product of self-assembly and were absent in the precipitate. They were not reproducible after the first heating, whereas endotherms at 204.5 and 247.7 °C remained reproducible; this indicates that **5b** adopts different molecular packing from the precipitate, which can be induced only by self-assembly with the phase transfer method.

On the contrary, **5c** showed similar thermal behavior in both precipitate and self-assembled nanofibers. Only one melting transition at 261.4 °C was observed from the precipitate of **5c**, which was reproducible with a slight decrease in temperature and heat of transition over repeated heating/cooling cycle. The melting point of the nanofibers

(22) (a) Terech, P.; Weiss, R. G. *Chem. Rev.* **1997**, *97*, 3133–3159. (b) Ajayaghosh, A.; Praveen, V. K. *Acc. Chem. Res.* **2007**, *40*, 644–656.

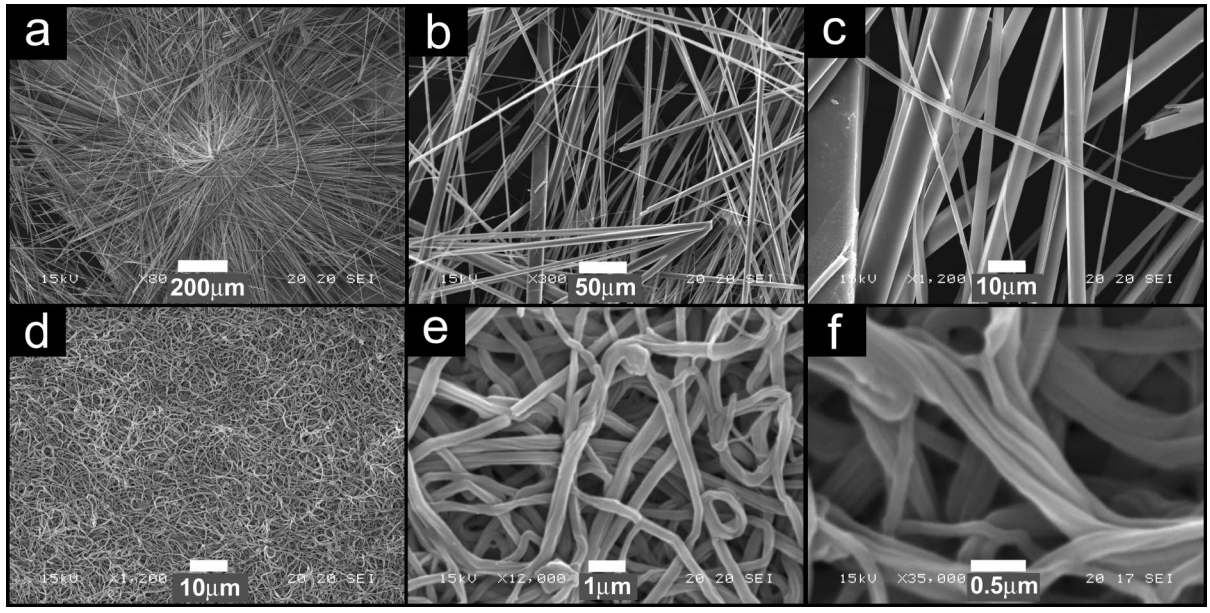

Figure 4. SEM images of microstrands of **5b** (a−c) and nanofibers of **5c** (d−f).

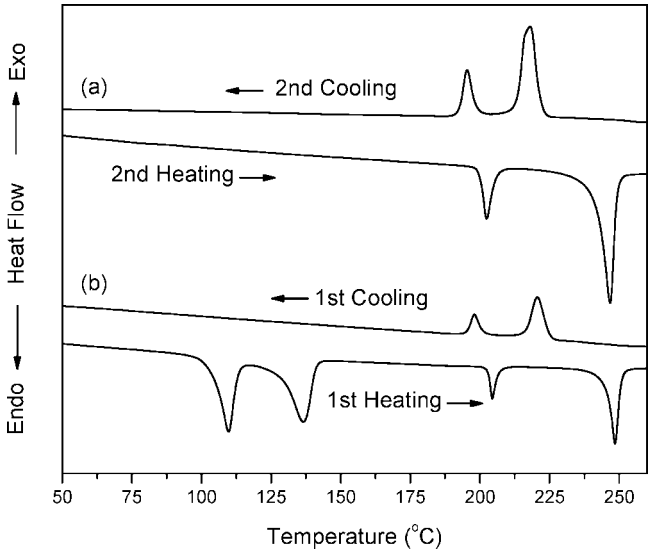

Figure 5. DSC thermograms of **5b**; (a) 2nd heating and cooling scans of precipitate, (b) 1st heating and cooling scans of microstrands.

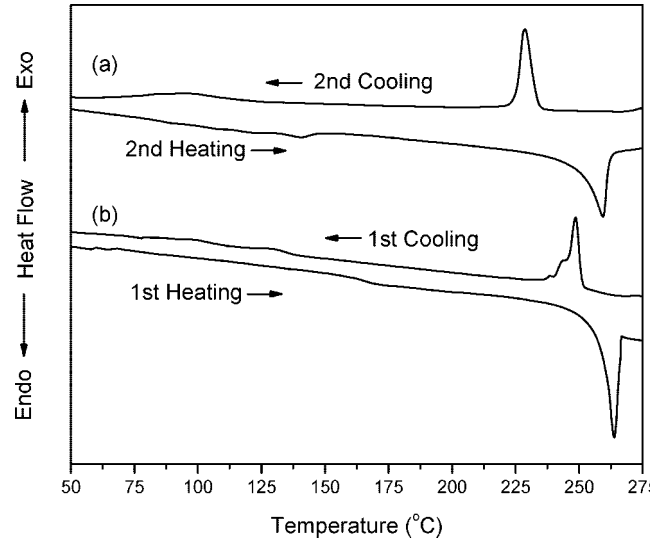

Figure 6. DSC thermograms of **5c**; (a) 2nd heating and cooling scans of precipitate, (b) 1st heating and cooling scans of nanofibers.

of **5c** was marginally different from that of precipitate, which may indicate similar molecular packing in both cases.

XRD measurements were used to investigate the molecular packing of the 1D assembled clusters (Figure 7). Again, as with DSC, precipitates of **5b** and **5c** were used as a control.

The XRD pattern of microstrands of **5b** showed considerable difference from the precipitate. The diffraction patterns of assembled **5b** exhibited defined peaks including $2\theta = 25°$ corresponding to a *d*-spacing of 3.5 Å, which is characteristic of an effective $\pi-\pi$ stacking distance.[2b,7a] On the other hand, the precipitate showed a broad peak which is attributed to the amorphous character of the sample. This result indicates that the growth of microstrands by intermolecular $\pi-\pi$ interaction is favored only when assembly condition such as solvent polarities and concentration is optimized. Note that the difference in the molecular packing of microstrands and precipitate of **5b** was also manifested by DSC. Meanwhile, the XRD patterns of both precipitate and nanofibers of **5c** showed a broad peak centered at 2θ = ca. 19° corresponding to a *d*-spacing of 4.7 Å, without noticeable diffraction at $2\theta = 25°$. The broad diffraction at the *d*-spacing of 4.7 Å has been reported as the stacking distance of coplanar π-conjugated polymer chains such as poly(9,9-dioctylfluorene)[23] and poly(2,7-carbazole) derivatives.[24]

Combined analyses of SEM, DSC, and XRD suggest that the formation of microstrands of **5b** and nanofibers of **5c** are driven by different intermolecular interactions. Although they are structural analogues, $\pi-\pi$ interaction is dominant in the case of **5b**, producing rigid straight microstrands, whereas such interaction plays a minor role in the case of **5c**. In the microstrands, molecules are assembling such that

(23) Grell, M.; Bradley, D. D. C.; Ungar, G.; Hill, J.; Whitehead, K. S. *Macromolecules* **1999**, *32*, 5810–5817.
(24) Blouin, N.; Michaud, A.; Gendron, D.; Wakim, S.; Blair, E.; Neagu-Plesu, R.; Belletête, M.; Durocher, G.; Tao, Y.; Leclerc, M. *J. Am. Chem. Soc.* **2008**, *130*, 732–742.

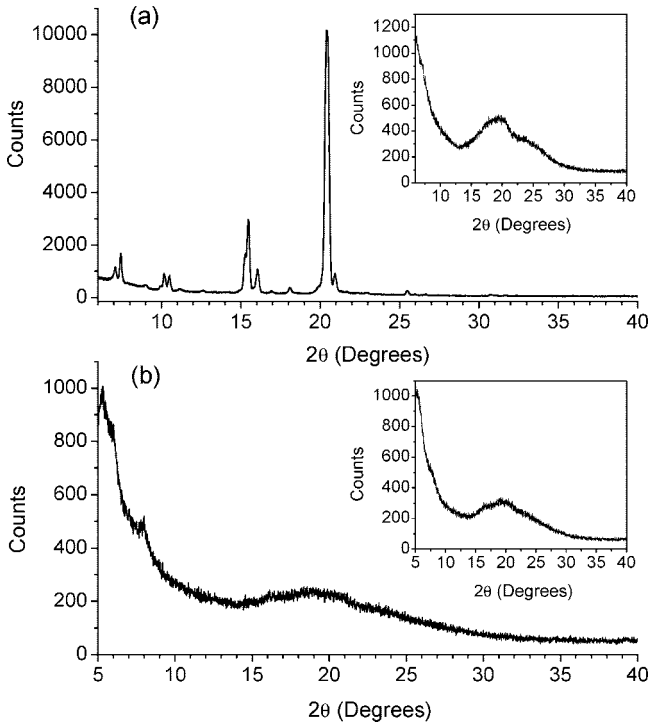

Figure 7. XRD powder patterns of (a) microstrands of **5b** and (b) nanofibers of **5c**. Both insets represent XRD powder patterns of precipitates of **5b** and **5c**, respectively.

$\pi-\pi$ stacking is the microstrands long axis direction, giving a well-resolved XRD pattern. On the other hand, such a crystalline XRD character is absent in the nanofibers of **5c**. This dramatic difference in assembling behavior of **5c** can be attributed to the presence of the cyanophenyl moiety. Cyanophenyl groups are known to have various and complex intermolecular interaction modes including cyano-phenyl and cyano-cyano (1D and 2D).[25] Under the assembly conditions employed in this work, intermolecular cyanophenyl interactions seem to be prevailing over $\pi-\pi$ interaction. Presumably, cyanophenyl moieties interact intermolecularly in the fiber long axis direction connecting the individual **5c** molecules. Further aggregation leads to the formation of flexible nanofibers in a similar way to the orientation of rigid conjugated polymers in the solid state, albeit lacking well-resolved diffraction as in the case of **5b**. A more detailed study on the effect of the cyanophenyl interactions on the morphologies of 1D assembly depending upon concentration and solvent polarities with infrared spectroscopy in conjunction with SEM and XRD is in progress.

(25) (a) Kuribayashi, M.; Hori, K. *Liq. Cryst.* **1999**, *26*, 809–815. (b) Hori, K.; Kuribayashi, M.; Iimuro, M. *Phys. Chem. Chem. Phys.* **2000**, *2*, 2863–2868.

Conclusions

We have demonstrated the validity of the new design strategy for developing T-shaped π-core molecules based on bisphenazine, incorporating tunable electronic properties while maintaining 1D self-assembling ability. More specifically, three important goals were achieved in this work: (1) T-shaped asymmetric bisphenazine π-cores were proved to be effective in self-assembly. (2) Although remote to the bisphenazine core, electronic properties of peripheral substituents (OCH_3, H, and CN) were clearly reflected in the reduction potential of the whole conjugated system. (3) The presence of soft intermolecular interaction of cyanophenyl moiety in the asymmetric bisphenazine modulated 1D assembling property producing flexible nanofibers while the absence of such interaction led to the formation of straight high-aspect-ratio microstrands via intermolecular $\pi-\pi$ interaction. The dramatic difference in the result from the assembly of **5b** and **5c** clearly shows that the 1D clusters were grown via different driving forces. The findings in this work give a great opportunity to control the electronic properties and the morphologies of 1D assembled clusters through a small variance in the molecular structure.

Acknowledgment. This work was partially supported by a Research Development Award from UNLV. Dr. Pradip K. Bhowmik and Dr. Haesook Han are greatly acknowledged for their help with thermal property analysis.

Supporting Information Available: Detailed syntheses, characterization, theoretical calculation, 1D self-assembly method, and polarized optical micrographs of 1D clusters and precipitates of **5b** and **5c** (PDF). This material is available free of charge via the Internet at http://pubs.acs.org.

CM800521P